# 1,4-Phenylenediacetate-Based Ln MOFs – Synthesis, Structures, Luminescence, and Catalytic Activity

## Yan-wei Ren,[a] Jia-xin Liang,[a] Jia-xian Lu,[a] Bo-wei Cai,[a,b] Da-bin Shi,[a] Chao-rong Qi,[a] Huan-feng Jiang,*[a] Jun Chen,[b] and De Zheng[b]

A series of new isostructural lanthanide MOFs, $[Ln_2(pda)_3(H_2O)] \cdot 2H_2O$ [Ln = La (**1**), Ce(**2**), Pr(**3**), Nd(**4**), Sm(**5**), Eu(**6**), Gd(**7**), Tb(**8**), Dy(**9**), Ho(**10**), Er(**11**), Tm(**12**), and Yb(**13**); $H_2dpa$ = 1,4-phenylenediacetate], have been solvothermally synthesized and structurally characterized by single-crystal (or/and powder) X-ray diffraction analysis. All the MOFs are isostructural and consist of 1D Ln–COO helixes that are cross-linked by the $-CH_2C_6H_4CH_2-$ spacers of the $pda^{2-}$ anions in a 3D compressed honeycomb-shaped network with 1D open channels, which accommodate guest and coordi-

nated water molecules. Evacuation of $[Ln_2(pda)_3(H_2O)] \cdot 2H_2O$ at 200 °C under vacuum generates $[Ln_2(pda)_3]$, which gives X-ray powder diffraction patterns consistent with those of $[Ln_2(pda)_3(H_2O)] \cdot 2H_2O$. MOFs **6** and **8** show characteristic luminescent properties. Activated $[Tb_2(pda)_3]$ exhibits excellent catalytic performance in the heterogeneous acetalization of benzaldehyde with methanol. The possibility for easy recycling makes this catalyst a highly promising candidate to address environmental concerns.

## Introduction

Recently, considerable attention has been devoted to the design and synthesis of metal–organic frameworks (MOFs) not only because of their interesting topological structures but also for their many potential applications in optoelectronics,[1] magnetic,[2] and porous materials.[3] MOFs or coordination polymers, are constructed by metal ions/clusters that are linked by organic ligands and belong to an interesting class of functional micro-and mesoporous materials.[4] The size of periodic pores/channels in MOFs and their functionality may be altered and tuned in a systematic way by choosing suitable metal ions and organic linkers.[5] One important feature of porous MOFs with open channels is that guest species can be removed and reintroduced reversibly without collapse of the framework.[6] As a result of the porous nature and structural stability of MOFs, efforts have been made towards imparting catalytic properties on to MOFs for heterogeneous catalysis.[7] Using metal ions in the framework as active centers for catalysis is one of the most common ways to generate catalytically active MOFs.[8] In addition, immobilization of metal complexes within the MOFs to create heterogeneous catalysts has also been reported.[9] Notably, some of the reported MOF catalysts also showed size selectivity.[10]

MOFs based on lanthanide ions have attracted great interesting during the past decade, primarily for their luminescent and magnetic properties.[1,2] Lanthanide-based MOFs have great potential to be excellent heterogeneous catalysts as lanthanide ions have variable coordination numbers (6–12), flexible coordination environments, and can manage coordinatively unsaturated metal centers.[11] There are some reports of the use of lanthanide-based MOFs as catalysts.[12] In order to search for new lanthanide-based MOF catalysts, we have focused our attention on a family lanthanide-based MOFs constructed from 1,4-phenylenediacetate ($H_2pda$), which heretofore has less been utilized in supporting Ln MOFs.[13] In comparison with 1,4-benzenedicaboxylate, $H_2pda$ has two secondary carbon atoms ($CH_2$) that connect two flexible carboxylate groups, consequently constructing porous lanthanide coordination polymers with less condensed and more open frameworks. Two such isostructural MOFs have been reported, $[La_2(pda)_3(H_2O)] \cdot 2H_2O$ and $[Er_2(pda)_3(H_2O)] \cdot 2H_2O$.[13a] These two MOFs contain 1D channels and show high thermal stability (200–450 °C). The coordinated and uncoordinated water molecules in the channels can be removed by evacuation and heating to form permanent pores, and, more significantly, dehydrated $[Er_2(pda)_3]$ can adsorb $CO_2$ but not Ar or $N_2$ into its pores.

The selective gas sorption of pda-based Ln MOFs, their porous nature, and structural flexibility prompted us to make a systematic study of this family of Ln MOFs and their potential as heterogeneous Lewis acid catalysts. In this paper, we report the synthesis, structures, photoluminescence, and catalytic activities of a series of new homoframe-

[a] School of Chemistry and Chemical Engineering,
South China University of Technology,
Guangzhou, 510640, China
E-mail: jianghf@scut.edu.cn
[b] Guangdong Winner Functional Materials Co., Ltd.,
Foshan, 528521, China

work lanthanide-based MOFs, $[Ln_2(pda)_3(H_2O)]\cdot 2H_2O$ [Ln = La (**1**), Ce(**2**), Pr(**3**), Nd(**4**), Sm(**5**), Eu(**6**), Gd(**7**), Tb(**8**), Dy(**9**), Ho(**10**), Er(**11**), Tm(**12**), Yb(**13**)], which are coordination isomers of the previously reported pda-based Ln MOFs.[13a] These lanthanide-based MOFs were characterized by X-ray powder diffraction (XRPD), and the structures of **6**, **7**, and **8**, as representative examples, were determined by single-crystal X-ray diffraction. The framework stability of **6** and **8** under dehydration and rehydration were further studied by XRPD. The catalytic performance of the lanthanide-based MOFs in terms of activity, heterogeneity, and reusability were tested in the acetalization of benzaldehyde with methanol.

## Results and Discussion

### Synthesis and Structures

Treatment of lanthanide(III) nitrate and 1,4-phenylenediacetate in dimethylacetamide and water inside a Teflon®-lined autoclave at 105 °C for 2 d yielded needle-shaped crystals of $[Ln_2(pda)_3(H_2O)]\cdot 2H_2O$. The crystalline solids are stable in air and insoluble in water and common organic solvents such as methanol, acetone, and DMF.

As representative examples, **6**, **7**, and **8** were measured by single-crystal X-ray diffraction to study their crystal structures, and the results revealed that these three MOFs are isostructural with a 3D framework. Thus, only the structure of **6** is described in detail. As shown in Figure 1, Eu1 is coordinated by nine oxygen atoms from one bis(monodentate) bridging carboxylate group (O3), two $\kappa^2$-$\kappa^1$-$\mu_2$-mode chelating carboxyl groups (O1 and O2, O11 and O12), three $\kappa^1$-$\kappa^2$-$\mu_2$-mode chelating carboxyl groups (O5, O7, and O10), and one coordinated water molecule (O1w). The nine oxygen atoms coordinated to Eu2 are from one bis(monodentate) bridging carboxylate group (O4), two $\kappa^1$-$\kappa^2$-$\mu_2$ mode chelating carboxyl groups (O1 and O11#2), and three $\kappa^2$-$\kappa^1$-$\mu_2$ mode chelating carboxyl groups (O5 and O6, O7 and O8, O9 and O10#3). The coordination environment of the two crystallographically independent europium ions is best described as distorted tricapped trigonal prism. The Eu–O (carboxylate) bond lengths range from 2.374(3)–2.688(3) Å, and the Eu–O (water) bond length is 2.445(4) Å,

all of which are within the range of those observed for other Eu$^{III}$ complexes with oxygen donor ligands.[13b,14]

In the polymeric structure of **6**, the Eu$^{III}$ ions are interconnected through COO$^-$ groups, forming 1D Eu–COO helices (–Eu1–Eu2–Eu1–Eu2–) that extends in the *c* direction (Figure 2 bottom). Three COO$^-$ groups bridge two adjacent Eu1 and Eu2 ions in one bis(monodentate) *syn–syn* mode ($\kappa^1$-$\kappa^1$-$\mu_2$) and two tridentate ($\kappa^2$-$\kappa^1$-$\mu_2$) bonding modes. Moreover, Eu2 and the adjacent Eu1#1 ion are bridged by three COO$^-$ groups with tridentate ($\kappa^2$-$\kappa^1$-$\mu_2$) bonding modes. These coordination types of the COO$^-$ group and node Eu$^{III}$ ions result in a 1D chain containing two interconnected subunits: the Eu$_2$O$_4$ subunit (Eu1–Eu2) with an edge-sharing polyhedron and the Eu$_2$O$_3$ subunit (Eu2–Eu1#1) with a trigonal plane-sharing polyhedron. The Eu···Eu diatance and two Eu–O–Eu angles within the Eu$_2$O$_4$ subunit are 4.144 Å, 105.76, and 113.77°, respectively. In comparison, the Eu···Eu diatance (3.948 Å) in the
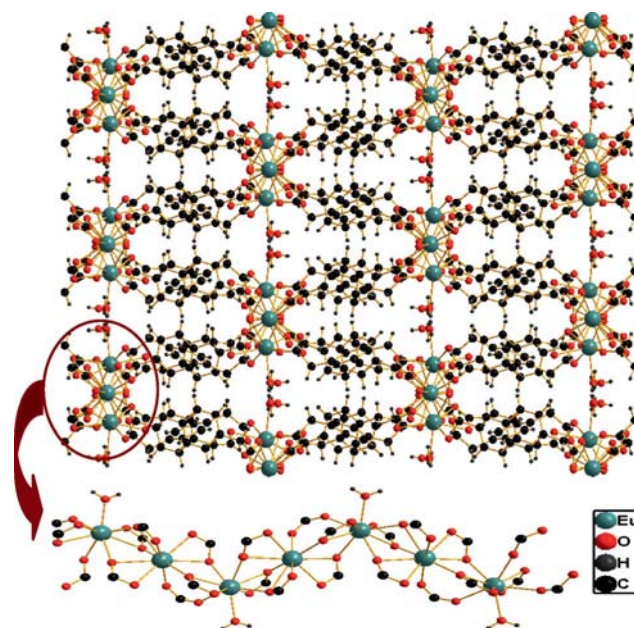


Figure 2. Representation of the extended 2D structure of **6** (top) and a fragment of the Eu–COO helix along the *c* direction (bottom).
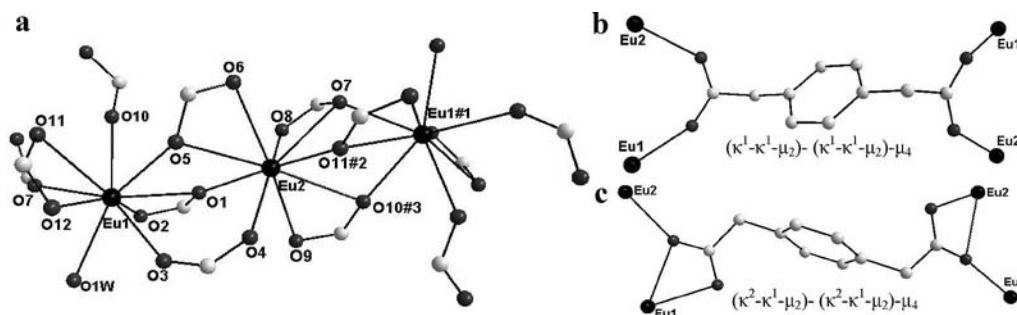


Figure 1. (a) Ball-and-stick representation of coordination environments of the two crystallographically independent Eu1 and Eu2 ions in **6**. Symmetry transformations used to generate equivalent atoms: #1 *x*, –*y* + 1/2, *z* + 1/2; #2 –*x* + 1, –*y*, –*z* + 2; #3 –*x* + 2, *y* + 1/2, –*z* + 3/2. (b) and (c) coordination modes of dpa$^{2–}$.

Eu$_2$O$_3$ subunit is shorter, and the three Eu–O–Eu angles are smaller (99.66, 100.42, and 103.19°). These 1D infinite helices may be viewed as supramolecular secondary building blocks, which are further cross-linked by the –CH$_2$C$_6$H$_4$CH$_2$– spacers of pda$^{2–}$ (Figures 1, b and c) into a 3D network, exhibiting a compressed honeycomb shape with 1D open channels (Figure 2). The two crystalline water molecules are located in the channels, and the coordinated water molecule points away from the Eu–pda framework and into the channel as result of extensive hydrogen interactions with the host skeleton. A PLATON calculation yields a solvent-accessible void volume of 307.2 Å$^3$ per unit cell (3162.6 Å$^3$), amounting to 9.7% of the crystal lattice (free guest removal). All water molecules can be removed upon heating in vacuo, and the free diameter of the circular channel is about 3.4 Å. Two coordination isomers [Ln$_2$(pda)$_3$(H$_2$O)]·2H$_2$O (Ln = La, Er) with similar unit cell parameters and identical space groups to our MOFs have been synthesized under high temperature hydrothermal conditions.[13a] Differently, in the two reported MOFs, the dpa$^{2–}$ ligand has four coordination modes bridging two crystallographically independent Ln$^{III}$ ions, and the coordination numbers of the two Ln$^{III}$ ions are eight and nine, respectively. These configurable differences further demonstrate the ability of lanthanide ions to have variable coordination numbers and flexible coordination environments.

In order to obtain more insight about the structural evolution of the family of pda-based Ln MOFs, the unit cell parameters of different MOFs obtained from single-crystal X-ray diffraction were compared with the atomic numbers for the corresponding Ln$^{III}$ ions (Figure 3 and Table S1 Supporting Information). The unit cell dimensions (a, b, and c) decrease nonlinearly with increasing atomic number (and decreasing ionic radii) of the Ln$^{III}$ ions, showing a distinct quasitetrad effect in the rare earth distribution patterns. Furthermore, same pattern is also observed for unit cell volume (V) vs. the atomic number of the Ln$^{III}$ ion. The structures of **6** and **8** refined from single-crystal X-ray diffraction data show that the average Tb–O distance [2.448(4) Å] is shorter than that of average Eu–O bond [2.517(3) Å], resulting in smaller a and V parameters. Recently a case was reported by Martín-Matute and Zou where the a (and b) parameters decrease linearly with the decreasing ionic radius of the Ln$^{III}$ ion for a family of [Ln(btc)(H$_2$O)] MOFs (btc = 1,3,5-benzenetricarboxylic acid).[12d] Combining the similarity of the XRPD patterns (Figure S1, Supporting Information), elemental analyses (C and H), and IR spectra of **1–13**, we can confirm that this family of Ln MOFs are homotypic.

## Thermal Properties

Thermogravimetric analysis (TGA) of **6** and **8**, as representative examples, has been carried out in the range of 25–1000 °C, and show similar behavior (Figure 4 and Figure S2 in the Supporting Information). From room temperature to about 200 °C, the two MOFs lose about 5.8% of their
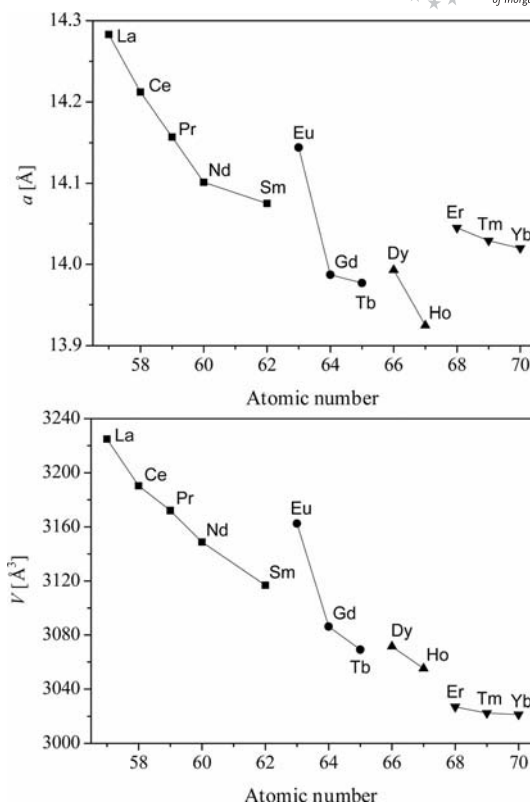


Figure 3. Unit cell parameters a (top) and V (bottom) of **1–13**, obtained from single-crystal X-ray diffraction, compared with the atomic number of Ln$^{III}$ ions.

initial weight, corresponding to the loss of noncoordinated and coordinated water molecules (calculated: 5.78 and 5.69% for **6** and **8**, respectively). A distinction between the coordinated and uncoordinated water molecules was not clearly observed from the TGA data. This result is in agreement with the presence of strong hydrogen bonds between the coordinated and the solvated water molecules. No further weight loss was found until approximately 450 °C, where the decomposition of [Ln$_2$(pda)$_3$] occurred, as indicated by a significant weight loss. No attempt was made to identify the products of decomposition.
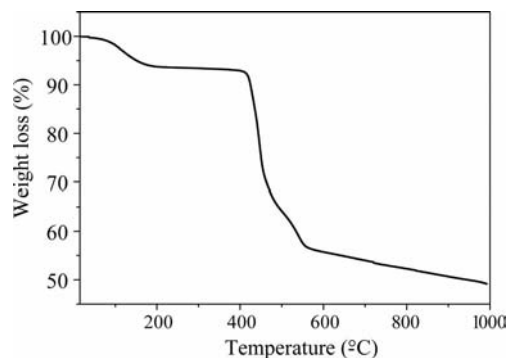


Figure 4. TG curve of **6**.

To investigate if these materials are robust to guest removal, their dehydration and rehydration were studied and XRPD was used to check the phases. Assisted by TGA

measurements, a representative preparative-scale sample of **6** was heated at 200 °C under vacuum, causing the loss of three water molecules per formula unit. The resulting solid [$Eu_2(pda)_3$] retains the framework and crystallinity observed in the original **6**, as supported by the consistent XRPD patterns of the two substances (Figure 5), which indicate that accessible metal sites can be obtained by removal of noncoordinated and coordinated water molecules after thermal activation. Furthermore, according to the TGA curve, after 200 °C, a long plateau appears and **6** is thermally stable up to over 450 °C, followed by the collapse of the framework. Generally, degradation of the organic components of MOFs typically starts at moderate temperatures (200–350 °C),[15] leading to the decomposition of the organic ligands. Only limited MOFs have been reported to be stable above 350 °C and the detailed reasons for this still remain unclear,[15,16] although it is usually accepted that Si- and Zr-based MOFs have higher thermal stablity.[16d] It has also been considered that the compact networks of the host frameworks could play a crucial role in determining their thermal stabilities. So far, of the rarely reported carboxylate-based MOFs with thermal stabilities higher than 450 °C, almost all have few accessible void spaces.[16] Therefore, **1**–**13** represent good examples of porous crystalline and structurally well-defined lanthanide–organic frameworks with ancillary ligands totally removed and Lewis-acidic metal sites opened, which may facilitate their application in catalysis. It is assumed that the strong eight- and nine-coordinate $Ln^{III}$–carboxylate interactions (bridging and chelating modes) tighten the backbone of the ligand to enhance their resistance to pyrolysis.
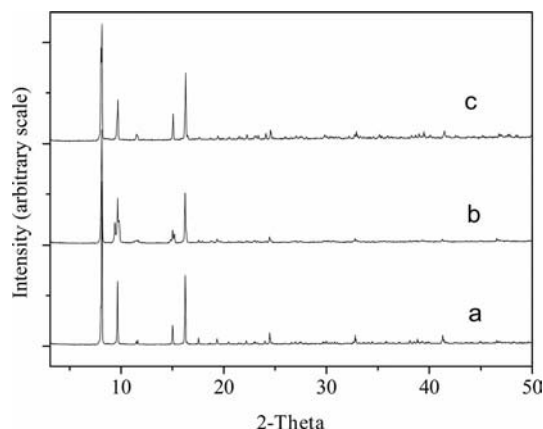


Figure 5. XRPD patterns: as-synthesized **6** (a), dehydrated [$Eu_2(pda)_3$] (b), and rehydrated **6** (c).

When the dehydrated [$Ln_2(pda)_3$] was immersed in water at room temperature for one day, it adsorbed water to recover the original [$Ln_2(pda)_3(H_2O)$]·$2H_2O$ structure, as indicated by comparing the XRPD patterns to those of the as-prepared samples (Figures 5 and 6). Consequently, dehydration and rehydration are reversible for these materials, and the frameworks show dynamics upon de-/rehydration. This is similar to the behavior of other previously reported Ln MOFs.[13a,14b,17]
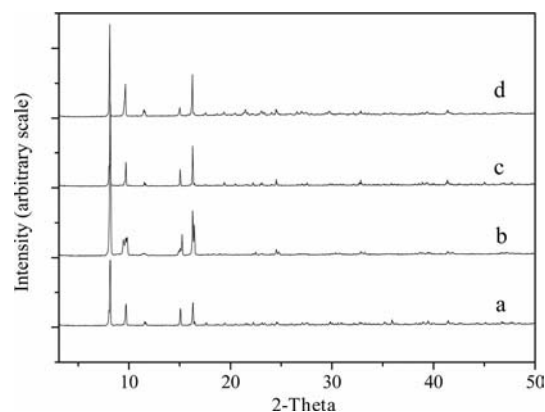


Figure 6. XRPD patterns: as-synthesized **8** (a), dehydrated [$Tb_2(pda)_3$] (b), rehydrated **8** (c), and [$Tb_2(pda)_3$] used three times in catalysis (d).

## Photoluminescent Properties of 6 and 8

Lanthanide complexes are known for their photoluminescent properties. The solid state photoluminescence spectra of **6** and **8** were recorded at room temperature and are depicted in Figures 7 and 8, respectively. The emission spec-



Figure 7. Solid-state emission spectra for **6** at room temperature upon excitation at 465 nm. Inset: solid state excitation spectra monitored at $\lambda_{em}$ = 618 nm.
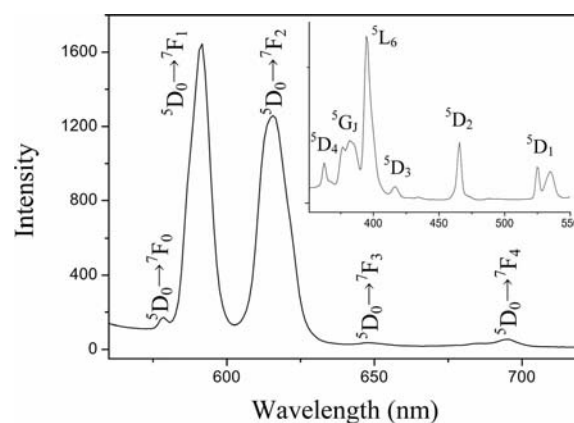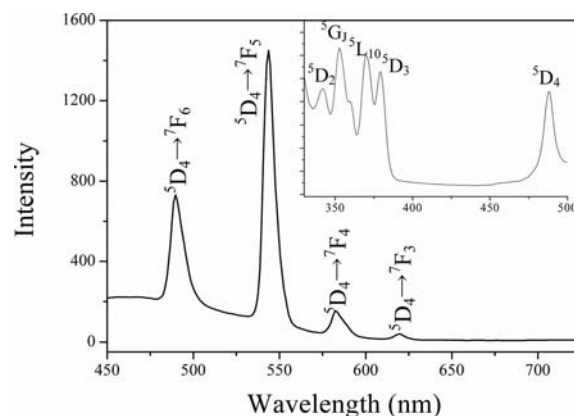


Figure 8. Solid-state emission spectra for **8** at room temperature upon excitation at 370 nm. Inset: solid state excitation spectra monitored at $\lambda_{em}$ = 544 nm.

tra of **6** upon excitation at 465 nm exhibits characteristic peaks at 578, 592, 618, 642, and 690 nm originating from the $^5D_0 \rightarrow {}^7F_J$ ($J = 0–4$) transition of the Eu[III] ion.[14] According to the selection rules for electric dipole transition, the appearance of the symmetry forbidden emission $^5D_0 \rightarrow {}^7F_0$ at 578 nm indicates that the Eu[III] ion possesses a noncentrosymmetric coordination environment. The $^5D_0 \rightarrow {}^7F_2$ electron dipole transition, the so-called hypersensitive transition, responsible for the brilliant-red emission of these complexes, is slightly weaker than the $^5D_0 \rightarrow {}^7F_1$ magnetic dipole transition, indicating a relatively unpolarizable chemical environment around the Eu[III] ion. These results are in good agreement with the crystallographic analysis of **6**. MOF **8** emits hypersensitive green light when excited at 370 nm, and gives a typical Tb[III] emission spectrum. The narrow, strong peaks at 490, 545, 582, and 620 nm were ascribed to the characteristic emissions of Tb[III] corresponding to electronic transitions from the excited state $^5D_4$ to the multiplets $^7F_J$ ($J = 6–3$), respectively.[14] The excitation spectra of **8** was monitored with the Tb[III] $^5D_4 \rightarrow {}^7F_J$ (544 nm) transition, and the line bands between 300 and 500 nm can be attributed to $^7F \rightarrow {}^5D_0$, $^7F \rightarrow {}^5L_{10}$, and $^7F \rightarrow {}^5G$ intraconfiguration forbidden $4f^8 \rightarrow 4f^8$ transitions of the Tb[III] ion.
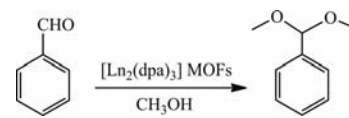
It is well known that the role of the triplet state of the ligand is very important for intramolecular energy transfer from the triplet state to the resonance level of a lanthanide ion. The photoluminescence spectra of **6** and **8** exhibit emission bands characteristic of the corresponding luminescent lanthanide ions, whereas the emissions arising from the free ligand H$_2$pda are not observed in the two MOFs (when excited at 357 nm, H$_2$pda exhibits two bands at 460 and 478 nm assigned to the $\pi^* \rightarrow \pi$ transition of the ligand).[18] The absence of ligand-based emission suggests efficient energy transfer from the ligand to the resonance level of the lanthanide ions during photoluminescence. These results indicate that the dpa$^{2-}$ ligands are capable of converting energy efficiently to the lanthanide centers, therefore, acting as efficient sensitizers of MOFs luminescence. Although more detailed theoretical and spectroscopic studies are necessary for a better understanding of the luminescence mechanism, the strong fluorescence emissions of **6** and **8** make them potentially useful photoactive materials.

## Catalytic Tests

To investigate the Lewis acid properties as catalysts of the pda$^{2-}$-based Ln MOFs, we choose the acetalization of aldehyde with methanol. Five representative MOF catalysts (10.0 mol-% for aldehyde), **1**, **4**, **6**, **8**, and **13**, were activated at 200 °C under vacuum for 4 h to generate coordinatively unsaturated Ln[III] centers and subsequently cooled down to room temperature under a nitrogen atmosphere. Benzaldehyde was selected as a model substrate and its acetalization reaction by methanol as a solvent and reagent in the presence of catalyst was screened with the aim of achieving high conversions. The results obtained for the transformation of

benzaldehyde with methanol to 1,1-dimethoxytoluene are shown in Table 1. The only product observed in this reaction is the corresponding dimethyl acetal, whereas hemiacetal was not found, probably due to the unfavorable formation equilibrium. A blank control shows that formation of a small quantity of 1,1-dimethoxytoluene ($< 2\%$) occurs when the reaction between benzaldehyde and methanol is performed in the absence of catalyst. It was found that [Tb$_2$(dpa)$_3$] shows very high activity with 78% conversion in 10 h (Table 1, entry 7). A higher conversion was reached at longer reaction times, however with only a minor increase in yield (Table 1, entry 8). Under the same conditions, other Ln MOF catalysts unexpectedly afforded quite low yields even with extended reaction times (entry 6, Table 1) despite being homotypic with [Tb$_2$(dpa)$_3$] (vide supra). In one previous case for heterogeneous Ln MOF catalysts in the cyanosilylation of aldehydes, the activity decreases due to the effect of lanthanide contraction,[12d] whereas in some cases for homogeneous lanthanide triflate [Ln(OTf)$_3$] catalysts, the relative Lewis acidities of Ln[III] increase.[19] However, the detailed reasons for the distinct catalytic activities of our pda-based Ln MOFs are still not clear in the acetalization of benzaldehyde with methanol.

Table 1. Acetalization of benzaldehyde with methanol using a variety of [Ln$_2$(dpa)$_3$] MOFs.[a]



| Entry | Catalyst | Time [h] | Conversion [%][b] |
|-------|----------|----------|-------------------|
| 1 | – | 10 | < 2 |
| 2 | [La$_2$(dpa)$_3$] | 10 | < 5 |
| 3 | [Nd$_2$(dpa)$_3$] | 10 | < 5 |
| 4 | [Eu$_2$(dpa)$_3$] | 10 | 26 |
| 5 | [Yb$_2$(dpa)$_3$] | 10 | 35 |
| 6 | [Yb$_2$(dpa)$_3$] | 20 | 56 |
| 7 | [Tb$_2$(dpa)$_3$] | 10 | 78 |
| 8 | [Tb$_2$(dpa)$_3$] | 24 | 84 |
| 9 | [Tb$_2$(dpa)$_3$] | 10 | 75,[c] 73,[d] 70[e] |
| 10 | [Tb$_2$(dpa)$_3$] | 10 | 22[f] |
| 11 | Tb(NO$_3$)$_3$·6H$_2$O | 10 | trace |

[a] Reaction conditions: benzaldehyde (1 mmol), catalyst (100 mg), and methanol (3 mL), room temperature. [b] Determined by GC–MS. [c] Yield of first reuse. [d] Yield of second reuse. [e] Yield of third reuse. [f] Reaction was performed in the presence of water (100 μL).

To provide evidence in favor of the Lewis acidic nature of the coordinatively unsaturated sites, a control experiment using [Tb$_2$(dpa)$_3$] was performed in the presence of about twenty times the stoichiometric amount of water with respect to the Tb[III] ions present in the catalyst for the acetalization of benzaldehyde with methanol as described in Table 1. The conversion of benzaldehyde under these conditions is only 22% after 10 h and this dramatic decrease in conversion is in agreement with the poisoning of [Tb$_2$-(dpa)$_3$] active sites by the coordination of water molecules to Tb[III] ions. This result also confirms that dehydration and rehydration are reversible for these Ln MOFs. Under the

same conditions, using **8** without dehydration shows no activity for this acetalization reaction. These experiments clearly demonstrate that the Lewis acidic nature of the coordinatively unsaturated sites is responsible for the catalytic process. For the sake of comparison, terbium nitrate hexahydrate, which has a similar terbium content as [Tb$_2$-(dpa)$_3$], was used as a homogeneous catalyst to probe Tb$^{III}$ as Lewis acidic sites for this reaction (entry 11, Table 1). However, there was no formation of 1,1-dimethoxytoluene after 10 h, indicating that the activity of Tb$^{III}$ as a Lewis acid in the homogeneous phase is diminished for this catalytic reaction.

The major advantage of the use of heterogeneous catalysts is the possible recovery of the catalyst from reaction mixtures and its reuse, particularly for industrial and pharmaceutical applications. To verify if [Tb$_2$(dpa)$_3$] decomposes and metal ions are leached out from the solid catalyst during reaction, the liquid phase of the reaction mixture was collected by filtration after about 50% formation of 1,1-dimethoxytoluene (after 3 h, Figure 9). The reaction solution in the absence of solid was again stirred at room temperature. After 24 h, the product formation was remeasured, and no obvious additional products were observed (Figure 9), which excludes the presence of an active catalytic species in the solution. Furthermore, XRPD and IR characterization were performed to check the stability of the catalyst. After the catalytic reactions were complete, the solid catalyst was recovered by filtration, washed several times with acetone, and dried under a nitrogen atmosphere. The recovered catalyst was then subjected to XRPD and IR analysis (Figures 6 and 10). Comparison of the XRPD and IR patterns of the pristine MOF and recovered catalyst convincingly demonstrate that the structural integrity of [Tb$_2$(dpa)$_3$] remains unaltered during the acetalization reaction. Notably the recovered catalyst can be reused several times for the acetalization reaction under identical conditions with no considerable loss of activity (entry 9, Table 1). The catalytic capability of [Tb$_2$(dpa)$_3$] for this reaction compares to that of the porous MOF [Cu$_3$(btc)$_2$] (HKUST-1) whose structure is constituted by clusters of two copper ions coordinated by four carboxylate groups of organic lin-

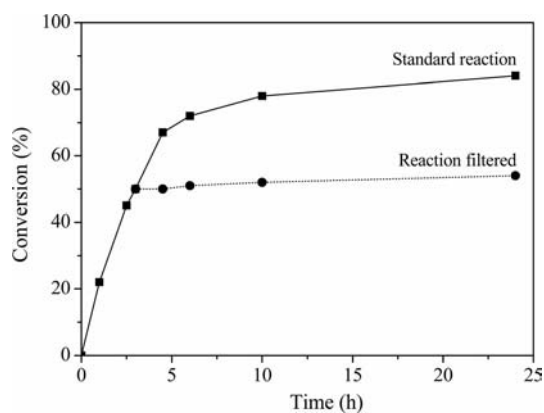kers with one free position available for each Cu$^{II}$ ion [under the same reaction conditions, the conversion of benzaldehyde catalyzed by {Cu$_3$(btc)$_2$} is 88% after 24 h].[20] The possibility of easy recycling makes these stable porous MOFs promising candidates for addressing environmental concerns.
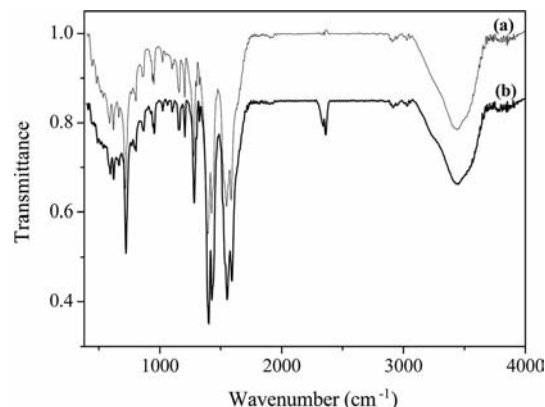


Figure 10. IR spectra of [Tb$_2$(pda)$_3$] (a) fresh and (b) recovered catalyst.

## Conclusions

We have successfully prepared a family of 3D isostructural lanthanide MOFs based on 1,4-phenylenediacetate with the formula [Ln$_2$(pda)$_3$(H$_2$O)]·2H$_2$O by a solvothermal route. Both the guest and the coordinated water molecules can be removed from the open channels, yielding porous [Ln$_2$(pda)$_3$], which maintain the framework and are stable up to 450 °C. The efficient energy transfer from the triplet state of pda$^{2-}$ to the resonance level of the lanthanide ions results in **6** and **8** exhibiting characteristic luminescent properties of Eu$^{III}$ and Tb$^{III}$ ions. These Ln MOFs also demonstrate the feasibility of achieving well defined, stable porous materials with coordinatively unsaturated metal sites such as [Tb$_2$(pda)$_3$], which exhibits excellent catalytic performance in heterogeneous acetalization of benzaldehyde with methanol. The catalytically active sites for this reaction are the Tb$^{III}$ ions acting as Lewis acids as demonstrated by the poisoning effect of coordinated water molecules. To the best of our knowledge, [Tb$_2$(dpa)$_3$] is the first lanthanide-based MOF that can efficiently catalyze the acetalization reaction of aldehyde with methanol under mild reaction conditions. This study affords new prospects for the design of lanthanide-based MOFs that can be used as recyclable heterogeneous acetalization catalysts. Further investigations employing this type of catalyst in other reactions are currently in progress.



Figure 9. Kinetic profiles for the conversion of 1,1-dimethoxytoluene catalyzed by [Tb$_2$(dpa)$_3$].

## Experimental Section

**Materials and Methods:** Lanthanide nitrates, 1,4-phenylenediacetate, and benzaldehyde were purchased from commercial suppliers and used without further purification. Methanol (HPLC grade) used in this work was commercial and the specified water content

was 0.02%. The C and H elemental analyses were performed with a Vario EL-III elemental analyzer. IR spectra were recorded with a Tensor-27 infrared spectrophotometer using KBr pellets (4000–400 cm$^{-1}$). XRPD patterns of the samples were obtained using a Bruker D8 ADVANCE powder diffractometer with Cu-$K_\alpha$ radiation at 40 kV and 40 mA at a step of 0.020. TGA were measured with a Q600 SDT instrument under N$_2$ (25–1000 °C, 10 °C/min). The luminescence spectra for the solid samples were measured at room temperature with a HITACHI F-4500 spectrophotometer with a xenon lamp as the light source. The products of the catalytic reactions were identified and quantified with a Finningan INC GC–MS.

**Synthesis of [{Ln$_2$(pda)$_3$(H$_2$O)}·2H$_2$O]$_n$ [Ln = La (1), Ce (2), Pr (3), Nd (4), Sm (5), Eu (6), Gd (7), Tb (8), Dy (9), Ho (10), Er (11), Tm (12), Yb (13)]:** Needle-shaped crystals were obtained by heating a mixture of Ln(NO$_3$)$_3$·6H$_2$O (0.4 mmol), 1,4-phenylendiacetate (116 mg, 0.6 mmol), distilled water (5 mL), and dimethylacetamide (5 mL) in a Teflon$^®$-lined 25 mL autoclave at 105 °C for 2 d, followed by slow cooling to room temperature. The yields, elemental analyses, and IR spectra of **6**, **7**, and **8** as representative examples are as follows. The phase purity of the all MOF bulk products were checked by comparing observed and simulated XRPD patterns.

**[{Eu$_2$(pda)$_3$(H$_2$O)}·2H$_2$O]$_n$ (6):** Yield 90% (based on H$_2$pda). C$_{30}$H$_{30}$Eu$_2$O$_{15}$ (934.48): calcd. C 38.25, H 3.17; found C 38.52, H 3.21. Main IR absorption bands (KBr): ṽ = 3448 (br), 1569 (br), 1432 (br), 1268 (s), 1220 (s), 1001 (s), 750 (s).

**[{Gd$_2$(pda)$_3$(H$_2$O)}·2H$_2$O]$_n$ (7):** Yield 86% (based on H$_2$pda). C$_{30}$H$_{30}$Gd$_2$O$_{15}$ (945.06): calcd. C 38.11, H 3.20; found C 38.09, H 3.17. IR (KBr): Main IR absorption bands (KBr): ṽ = 3450 (br), 1569 (br), 1433 (br), 1251 (s), 1220 (s), 1011 (s), 732 (s).

**[{Tb$_2$(pda)$_3$(H$_2$O)}·2H$_2$O]$_n$ (8):** Yield 84% (based on H$_2$pda). C$_{30}$H$_{30}$O$_{15}$Tb$_2$ (948.41): calcd. C 37.86, H 3.10; found C 37.96, H 3.16. IR (KBr): Main IR absorption bands (KBr): ṽ = 3449 (br), 1532 (br), 1419 (br), 1246 (s), 1222 (s), 1007 (s), 728 (s).

**X-ray Crystallography:** Unit cell parameters of all Ln MOFs were measured with a Rigaku R-AXIS SPIDER X-ray diffractometer using graphite-monochromated Mo-$K_\alpha$ radiation ($\lambda$ = 0.71073 Å) at 293 K. Reflection intensity data of **6**, **7**, and **8** as representative examples were collected in order to resolve their crystal structures. The structures were solved by direct methods and refined on $F^2$ by the full-matrix least-squares technique with SHELXTL-97.[21] The

hydrogen atoms were located at idealized positions using standard geometric criteria and treated with a riding model. The crystallographic data and the main bond lengths and angles are summarized in Table 2 and Table S2 in the Supporting Information, respectively.

CCDC-822486 (for **6**), -822487 (for **7**), and 822488 (for **8**) contain the supplementary crystallographic data for this paper. These data can be obtained free of charge from The Cambridge Crystallographic Data Centre via www.ccdc.cam.ac.uk/data_request/cif.

**Catalytic Studies:** Acetalization of benzaldehyde with methanol was used to study the catalytic performance of the [Ln$_2$(dpa)$_3$] MOFs as Lewis acid catalysts. Samples from the same synthesis batch were used for all the catalytic experiments. A MOF sample (about 10%) was activated in vacuo at 200 °C for 4 h to generate unsaturated lanthanide metal centers and then cooled down to room temperature under a nitrogen atmosphere. A solution of benzaldehyde (1 mmol) in methanol (3 mL) was added to the catalyst. The reaction mixture was stirred for the required time at room temperature. After the required reaction time, the reaction mixture was filtered and the products were analyzed by GC–MS. The recovered catalyst was washed with methanol, dried, and reused without further purification for the next run with fresh benzaldehyde with methanol.

**Supporting Information** (see footnote on the first page of this article): Selected bond lengths and angles for **6**, unit cell parameters and XRPD patterns of **1**–**13**, TGA curve of **8**.

[1] a) F. X. L. Xamena, A. Corma, H. Harcia, *J. Phys. Chem. C* **2007**, *111*, 80–85; b) Z. Liu, L. N. Sun, L. Y. Shi, D. S. Zhang, *Prog. Chem.* **2011**, *23*, 153–164; c) J. Rocha, L. D. Carlos, F. A. A. Paz, D. Ananias, *Chem. Soc. Rev.* **2011**, *40*, 926–940.

[2] M. C. Dul, E. Pardo, R. Lescouezec, Y. Journaux, J. Ferrando-Soria, R. Ruiz-Garcia, J. Cano, M. Julve, F. Lloret, D. Cangussu, C. L. M. Pereira, H. O. Stumpf, J. Pasan, C. Ruiz-Perez, *Coord. Chem. Rev.* **2010**, *254*, 2281–2296.

[3] D. Zhao, D. J. Timmons, D. Q. Yuan, H. C. Zhou, *Acc. Chem. Res.* **2011**, *44*, 123–33.

[4] a) S. L. James, *Chem. Soc. Rev.* **2003**, *32*, 276–288; b) J. L. C. Rowsell, O. M. Yaghi, *Microporous Mesoporous Mater.* **2004**, *73*, 3–14; c) M. J. Rosseinsky, *Microporous Mesoporous Mater.* **2004**, *73*, 15–30; d) G. Férey, *Chem. Soc. Rev.* **2008**, *37*, 191–214; e) S. L. Qiu, G. S. Zhu, *Coord. Chem. Rev.* **2009**, *253*, 2891–2911.

[5] a) O. M. Yaghi, M. O'Keeffe, N. W. Ockwing, H. K. Chae, M. Eddaoudi, J. Kim, *Nature* **2003**, *423*, 705–713; b) D. J. Tranchemontagne, J. L. Mendoza-Cortés, M. O'Keeffe, O. M. Yaghi, *Chem. Soc. Rev.* **2009**, *38*, 1257–1283.

[6] S. Natarajan, P. Mahata, *Chem. Soc. Rev.* **2009**, *38*, 2304–2318.

[7] a) B. Kesanli, W. B. Lin, *Coord. Chem. Rev.* **2003**, *246*, 305–326; b) S. Kitagawa, R. Kitaura, S. I. Noro, *Angew. Chem. Int. Ed.* **2004**, *43*, 2334–2375; c) H. L. Ngo, W. B. Lin, *Top. Catal.* **2005**, *34*, 85–92; d) D. Farrusseng, S. Aguado, C. Pinel, *Angew. Chem. Int. Ed.* **2009**, *48*, 7502–7513; e) J. Y. Lee, O. K. Farha,

Table 2. Crystal structure refinement data for **6**, **7**, and **8**.

| MOFs | 6 | 7 | 8 |
|---|---|---|---|
| Formula | C$_{30}$H$_{30}$O$_{15}$Eu$_2$ | C$_{30}$H$_{30}$O$_{15}$Gd$_2$ | C$_{30}$H$_{30}$O$_{15}$Tb$_2$ |
| Formula weight | 934.48 | 945.05 | 948.40 |
| $T$ [K] | 298 | 298 | 298 |
| Crystal system | monoclinic | monoclinic | monoclinic |
| Space group | $P2_1/c$ | $P2_1/c$ | $P2_1/c$ |
| $a$ [Å] | 14.144 | 13.987 | 13.977 |
| $b$ [Å] | 10.165 | 10.110 | 10.082 |
| $c$ [Å] | 22.005 | 21.835 | 21.787 |
| $\beta$ [°] | 91.548 | 91.623 | 91.491 |
| $V$ [Å$^3$] | 3162.6 | 3086.2 | 3069.1 |
| $Z$ | 4 | 4 | 4 |
| $D_{calcd}$ [g/cm$^3$] | 1.958 | 2.034 | 1.777 |
| $\mu$ [mm$^{-1}$] | 4.003 | 4.336 | 3.500 |
| Data / restr. / param. | 7191 / 2 / 420 | 7051 / 1 / 436 | 7000 / 0 / 436 |
| Final $R$ indices | $R_1 = 0.0297$ | $R_1 = 0.0237$ | $R_1 = 0.0311$ |
| [$I > 2\sigma(I)$] | $wR_2 = 0.0790$ | $wR_2 = 0.0502$ | $wR_2 = 0.0738$ |
| $R$ indices | $R_1 = 0.0324$ | $R_1 = 0.0301$ | $R_1 = 0.0341$ |
| (all data) | $wR_2 = 0.0812$ | $wR_2 = 0.0540$ | $wR_2 = 0.0751$ |

H.-f. Jiang et al.

J. Roberts, K. A. Scheidt, S. B. T. Nguyen, J. T. Hupp, *Chem. Soc. Rev.* **2009**, *38*, 1450–1459; f) Z. Wang, G. Chen, K. Ding, *Chem. Rev.* **2009**, *109*, 322–359.

[8] a) O. R. Evans, H. L. Ngo, W. B. Lin, *J. Am. Chem. Soc.* **2001**, *123*, 10395–10396; b) K. Schlichte, T. Kratzke, S. Kaskel, *Microporous Mesoporous Mater.* **2004**, *73*, 81–88; c) R. Q. Zou, H. Sakurai, Q. Xu, *Angew. Chem. Int. Ed.* **2006**, *45*, 2542–2546; d) L. Alaerts, E. Séguin, H. Poelman, F. Thibault-Starzyk, P. A. Jacobs, D. E. De Vos, *Chem. Eur. J.* **2006**, *12*, 7353–7363; e) S. Horike, M. Dincǎ, K. Tamaki, J. R. Long, *J. Am. Chem. Soc.* **2008**, *130*, 5854–5855; f) M. Wang, M. H. Xie, C. D. Wu, Y. G. Wang, *Chem. Commun.* **2009**, 2396–2398; g) M. Savonnet, S. Aguado, U. Ravon, D. Bazer-Bachi, V. Lecocq, N. Bats, C. Pinel, D. Farrusseng, *Green Chem.* **2009**, *11*, 1729–1732; h) W. Kleist, F. Jutz, M. Maciejewski, A. Baiker, *Eur. J. Inorg. Chem.* **2009**, 3552–3561; i) J. Gascon, U. Aktay, M. D. Hernandez-Alonso, G. P. M. van Klink, F. Kapteijn, *J. Catal.* **2009**, *261*, 85–87; j) P. K. Thallapally, C. A. Fernandez, R. K. Motkuri, S. K. Nune, J. Liu, C. H. F. Peden, *Dalton Trans.* **2010**, *39*, 1692–1694; k) D. B. Dang, Y. Bai, C. He, J. Wang, C. Y. Duan, J. Y. Niu, *Inorg. Chem.* **2010**, *49*, 1280–1282.

[9] a) C. D. Wu, A. Hu, L. Zhang, W. B. Lin, *J. Am. Chem. Soc.* **2005**, *127*, 8940–8941; b) L. Alaerts, J. Wahlen, P. A. Jacobs, D. E. De Vos, *Chem. Commun.* **2008**, 1727–1737; c) A. M. Shultz, O. K. Farha, J. T. Hupp, S. T. Nguyen, *J. Am. Chem. Soc.* **2009**, *131*, 4204–4205; d) F. J. Song, C. Wang, J. M. Falkowski, L. Q. Ma, W. B. Lin, *J. Am. Chem. Soc.* **2010**, *132*, 15390–15398.

[10] a) D. N. Dybtsev, A. L. Nuzhdin, H. Chun, K. P. Bryliakov, E. P. Talsi, V. P. Fredin, K. Kim, *Angew. Chem. Int. Ed.* **2006**, *45*, 916–920; b) S. H. Cho, B. Ma, S. T. Nguyen, J. T. Hupp, T. E. Albrechyschmitt, *Chem. Commun.* **2006**, 2563–2565; c) C. D. Wu, W. B. Lin, *Angew. Chem. Int. Ed.* **2007**, *46*, 1075–1078; d) D. M. Jiang, A. Urakawa, M. Yulikov, T. Mallat, G. Jeschke, A. Baiker, *Chem. Eur. J.* **2009**, *15*, 12255–12262.

[11] S. Kitagawa, S. I. Noro, T. Nakamura, *Chem. Commun.* **2006**, 701–707.

[12] a) J. W. Han, C. L. Hill, *J. Am. Chem. Soc.* **2007**, *129*, 15094–15095; b) F. Gándara, A. Garcia-Cortés, C. Cascales, B. Gómez-Lor, E. Gutiérrez-Puebla, M. Iglesias, A. Monge, N. Snejko, *Inorg. Chem.* **2007**, *46*, 3475–3484; c) F. Gándara, A. de Andrés, B. Gómezlor, E. Gutiérrez-Puebla, A. Monge, D. M. Proserpio, N. Snejko, *Cryst. Growth Des.* **2008**, *8*, 378–380; d) M. Gustafsson, A. Bartoszewicz, B. Martín-Matute,

J. L. Sun, J. Grins, T. Zhao, Z. Y. Li, G. S. Zhu, X. D. Zou, *Chem. Mater.* **2010**, *22*, 3316–3322; e) R. Sen, S. Koner, D. K. Hazre, M. Helliwell, M. Mukherjee, *Eur. J. Inorg. Chem.* **2011**, 241–248.

[13] a) L. Pan, K. M. Adams, H. E. Hernandez, X. T. Wang, C. Zheng, Y. Hattori, K. Kaneko, *J. Am. Chem. Soc.* **2003**, *125*, 3062–3067; b) P. C. R. Soare-Santos, L. Cunha-Silva, F. A. A. Paz, R. A. S. Ferreira, J. Rocha, T. Trindade, L. D. Carlos, H. I. S. Nogueira, *Cryst. Growth Des.* **2008**, *8*, 2505–2516.

[14] a) X. J. Wang, Z. M. Cen, Q. L. Ni, X. F. Jiang, H. C. Lian, L. C. Gui, H. H. Zuo, Z. Y. Wang, *Cryst. Growth Des.* **2010**, *10*, 2960–2968; b) Z. J. Lin, B. Xu, T. F. Liu, M. N. Cao, J. Lü, R. Cao, *Eur. J. Inorg. Chem.* **2010**, 3842–3849; c) G. Peng, Y. C. Qiu, Z. H. Liu, B. Liu, H. Deng, *Cryst. Growth Des.* **2010**, *10*, 114–121.

[15] a) D. X. Xue, J. B. Lin, J. P. Zhang, X. M. Chen, *CrystEngComm* **2009**, *11*, 183–188; b) Q. Gao, F. L. Jiang, M. Y. Wu, Y. G. Huang, W. Wei, M. C. Hong, *Cryst. Growth Des.* **2010**, *10*, 184–190.

[16] a) J. Perles, M. Iglesias, M. A. Martin-Luengo, M. A. Monge, C. Ruiz-Valero, N. Snejko, *Chem. Mater.* **2005**, *17*, 5837–5842; b) D. T. DeLii, C. L. Cahill, *Chem. Commun.* **2006**, 4946–4948; c) R. Q. Zou, R. Q. Zhong, M. Du, T. Kiyobayashi, Q. Xu, *Chem. Commun.* **2007**, 2467–2469; d) S. Bordiga, K. P. Lillerud, *J. Am. Chem. Soc.* **2008**, *130*, 13850–13851; e) D. Banerjee, L. A. Borkowski, S. J. Kim, J. B. Parise, *Cryst. Growth Des.* **2009**, *9*, 4922–4926; f) H. L. Jiang, N. Tsumori, Q. Xu, *Inorg. Chem.* **2010**, *49*, 10001–10006.

[17] a) A. Michaelides, S. Skoulika, *Cryst. Growth Des.* **2005**, *5*, 529–533; b) W. H. Zhu, Z. M. Wang, S. Gao, *Inorg. Chem.* **2007**, *46*, 1337–1342.

[18] T. F. Liu, J. Lü, L. X. Shi, Z. G. Guo, R. Cao, *CrystEngComm* **2009**, *11*, 583–588.

[19] a) S. Kobayashi, S. Nagayama, T. Busujima, *J. Am. Chem. Soc.* **1998**, *120*, 8287–8288; b) H. Tsuruta, T. Imamoto, K. Yamaguchi, *Chem. Commun.* **1999**, 1703–1704; c) M. Yamanaka, A. Nishida, M. Nakagawa, *Org. Lett.* **2000**, *2*, 159–161.

[20] A. Dhakshinamoorthy, M. Alvaro, H. Garciaa, *Adv. Synth. Catal.* **2010**, *352*, 3022–3030.

[21] G. M. Sheldrick, *SHELXTL-97*, *Crystal structure solution and refinement package*, University of Göttingen, Germany, **1997**.